

Cross Correlating Tidal Reconstructed 21cm Signal with Kinematic Sunyaev-Zel'dovich Effect: A New Probe for Missing Baryons at $z \sim 1 - 2$

Dongzi Li,^{1,2} Ue-Li Pen,^{3,4,5,1} Hong-Ming Zhu,^{6,7} and Yu Yu⁸

¹*Perimeter Institute for Theoretical Physics, 31 Caroline St. N., Waterloo, ON, N2L 2Y5, Canada*

²*University of Waterloo, 200 University Ave W, Waterloo, ON, N2L 3G1, Canada*

³*Canadian Institute for Theoretical Astrophysics, 60 St. George Street, Toronto, Ontario M5S 3H8, Canada*

⁴*Dunlap Institute for Astronomy and Astrophysics, 50 St. George Street, Toronto, Ontario M5S 3H4, Canada*

⁵*Canadian Institute for Advanced Research, CIFAR Program in Gravitation and Cosmology, Toronto, Ontario M5G 1Z8, Canada*

⁶*Key Laboratory for Computational Astrophysics, National Astronomical Observatories, Chinese Academy of Sciences, 20A Datun Road, Beijing 100012, China*

⁷*University of Chinese Academy of Sciences, Beijing 100049, China*

⁸*Key laboratory for research in galaxies and cosmology, Shanghai Astronomical Observatory, Chinese Academy of Sciences, 80 Nandan Road, Shanghai 200030, China*

(Dated: May 20, 2016)

The kinetic Sunyaev-Zel'dovich(kSZ) effect on Cosmic Microwave Background(CMB), induced by radial momentum of hot electrons, is a powerful source to probe baryon distributions. However, the signal is weak and lack of redshift information, hence another survey with spectroscopic redshift is typically required. This largely limits the sky area and depth to harness kSZ. Here, we propose a new source for cross correlation—HI density field from 21cm intensity mapping. 21cm spectra provide accurate redshift and intensity mappings integrate weak diffuse spectra, and thus can survey large sky area with great depth in much shorter time with low costs.

One main concern of the method is that the complicate 21cm foregrounds will contaminate radial large scale information, and reduce the correlation with kSZ. For redshift 1 and 2, we imitate the foreground subtraction in simulations, and find that after velocity reconstructions, there is $\gtrsim 0.5$ correlation with kSZ signal for $l \gtrsim 1000$, and it drops fast for $l < 1000$. To improve the behavior, we recover large scale modes from their tidal influence on small scale structures (Cosmic Tidal Reconstruction). Successfully recover $> 90\%$ information at $k \sim 0.01h/Mpc$, we obtain a new $r > 0.6$ correlation for $l \sim 100 - 2000$, which corresponds to $S/N > 3$ for $l \sim 500 - 3000$ with Planck noise. Since the reconstructed field and foreground subtracted field are superior in different modes, it is easy to combine them and get better S/N

PACS numbers:

I. INTRODUCTION

While the baryon abundance of early universe is well fixed [1–4], at $z \lesssim 2$ the detected baryon content in collapsed objects, eg. galaxies, galaxy clusters and groups, only account for 10% of the predicted amount. More baryons are believe to reside in Warm-Hot Intergalactic Mediums (WHIM) with typical temperature of 10^5 K to 10^7 K [5][6], which is too cold and diffuse to be detected. Continuous effort has been made to detect this part of baryons. One common approach is using hydrogen and metal absorption lines(eg, HI, Mg II, Si II, C II, Si III, C III, Si IV, O VI, O VII) [7][8]. However, the lines are usually limited to close circumgalactic medium, while at least 25% of the baryons are believed to reside in more diffused region [9]. Moreover, the uncertainty in metallicity would sometimes reduce the reliability.

A promising tool to probe the missing baryon is the kinetic Sunyaev-Zel'dovich(kSZ) effect [10][11], an effect that is greatly known for its potential to explore the Epoch of Reionization [12][13][14]. It refers to the secondary temperature anisotropy in CMB caused by Compton-scattering of CMB photon with free electrons. The radial velocity of electrons will give a Doppler shift to Since kSZ signal only relates to electron density and radial velocity, regardless the temperature and pressure, and velocity mainly results from large scale structure, the method is less biased towards hot, compact place, and provide more information on the fraction of diffused baryons.

Attractive as it is, due to the contamination of primary CMB, facility noises and probably residual thermal SZ signal, it is difficult to filter for the kSZ signal independently. Worse still, the signal itself does not contain redshift information.

To fix this, previous approaches cross correlated it with galaxy surveys, eg. using pairwise-momentum estimator [15] or velocity-field-reconstruction estimator [16][17]. However since they all require spectroscopy of galaxies to provide accurate redshift, the sky volume and redshift range to apply the method is limited. A recent effort try to fix this using projected fields of galaxies, which is cheap and feasible [18]. However, projected fields only make use of information from the largest scale in z direction, while for $l \gtrsim 1000$, where primary CMB fades away, a sufficient amount of kSZ signal comes from smaller scales. This limits the accuracy and S/N it can reach.

In this paper we put forward a new tracer for cross correlation—HI density field from 21cm intensity mapping. Density contrast from 21cm spectra have accurate redshift information, which enables us to reconstruct velocity field and get better correlation with kSZ powerspectra. Moreover, intensity mapping is a kind of surveys that integrates different signals, rather than distinguishing individual galaxies. It accumulates contributions from weak sources and hence be able to reach high S/N at shorter time. There are already several ongoing 21cm experiments aim at large sky coverage and claim to be able to reach $z \gtrsim 1$ in very near future. CHIME [19], Tianlai [20], HIRAX [21] etc. Therefore, this correlator is

more feasible than large galaxy spectroscopic surveys, and more accurate than projected field.

However, the 21cm density field has its own drawback—the complicated foregrounds results from integration. While a cosmic signal in 21cm measurement is of the order of mK, foregrounds coming from Galactic emissions, telescope noise, extragalactic radio sources and Radio recombination lines, can reach the order of Kelvin [22][23]. Lots of techniques have been developed to subtract the foregrounds, taking advantage of the attribute that they have fewer bright spectral degrees of freedom[24]. Unfortunately, subtraction will contaminate the smooth large scale structure information in radial direction. Since the kSZ signal coming from a both density and velocity field, and velocity is greatly related to large scale structures. This drawback will inhibit the cross correlation behavior.

In this paper, we first discuss the influence of foregrounds and small scale noises, based on simulation and analysis. To improve the correlation, we for apply a new method called 3D Cosmic Tidal Reconstruction [25][26], which recover the large scale modes of density field from its tidal influence on small scale structures.

The paper is organized as follows: In section II, we demonstrate given a density field, how to correlate with kSZ signal with velocity reconstruction; In section III, we present the result of cross correlation with foreground subtracted field and discuss the behavior; Then in section IV, we introduce the method of 3D tidal reconstruction, and present the correlation results after small k modes recovered, In section V, we estimate statistical errors, and we discuss and conclude at section VI.

Notes: Throughout the paper, We use the $z = 1, 2$ output of six N -body simulations from the CUBEP³M code [27], each evolving 1024^3 particles in a $(1.2\text{Gpc}/h)^3$ box. Simulation parameters are as follows: Hubble parameter $h = 0.678$, baryon density $\Omega_b = 0.049$, dark matter density $\Omega_c = 0.259$, amplitude of primordial curvature power spectrum $A_s = 2.139 \times 10^{-9}$ at $k_0 = 0.05 \text{ Mpc}^{-1}$ and scalar spectral index $n_s = 0.968$.

we use “ \wedge ” to denote reconstructed fields as oppose to fields directly from simulations.

II. VELOCITY RECONSTRUCTION AND KSZ SIGNALS CROSS CORRELATION

The CMB temperature fluctuations caused by kSZ effect is:

$$\Theta_{kSZ}(\hat{n}) \equiv \frac{\Delta T_{kSZ}}{T_{\text{CMB}}} = -\frac{1}{c} \int d\eta g(\eta) \mathbf{p}_{\parallel}, \quad (1)$$

where $\eta(z)$ is the comoving distance at redshift z , $g(\eta) = e^{-\tau} d\tau/d\eta$ is the visibility function, τ is the optical depth to Thomson scattering, $\mathbf{p}_{\parallel} = (1 + \delta)\mathbf{v}_{\parallel}$, with δ the electron overdensity. We assume that $g(\eta)$ doesn't change significantly in one redshift bin, and integrate \mathbf{p}_{\parallel} along radial axis to get $\hat{\Theta}_{kSZ}$.

Due to the cancellation of positive and negative velocity, its direct cross correlation between kSZ signal will vanish. To better maintain the one to one multiplication between velocity field and density contrast, we first calculate the linear peculiar

velocity, and then generate a mock kSZ signal [16]. In this way, we can at most maximize the correlation.

Assume we have a density contrast field $\delta = \frac{\rho - \bar{\rho}}{\bar{\rho}}$, where $\bar{\rho}$ is the average density of a certain redshift slice.

Detailed steps are as follows.

(1) Estimate the velocity field:

In linear region, the continuity equation goes like: $\dot{\delta} + \nabla \cdot \mathbf{v} = 0$, where \mathbf{v} is the peculiar velocity and δ is the matter overdensity.

Therefore, we obtain an estimator of velocity distribution from the density contrast δ :

$$\hat{v}_z(\mathbf{k}) = iaHf\delta(\mathbf{k})\frac{k_z}{k^2} \quad (2)$$

where $f = \frac{d \ln D}{d \ln a}$, $D(a)$ is the linear growth function, a is the scale factor, H is the Hubble parameter.

$v_z \propto \frac{k_z}{k^2}$, indicating the most prominent signal comes from small k mode, which corresponds to large scale structure.

(2) suppress the noise in velocity field with a Wiener filter. This is because the term $\frac{k_z}{k^2}$ in Eq.(2) will strongly amplify noises in small k modes.

$$\hat{v}_z^c(\mathbf{k}) = \frac{\hat{v}_z(\mathbf{k})}{b(k_{\perp}, k_{\parallel})} W(k_{\perp}, k_{\parallel}), \quad (3)$$

Bias $b = \frac{P_{\hat{v}_z, v_z}}{P_{v_z}}$, Wiener filter $W = \frac{P_{v_z}}{P_{\hat{v}_z}/b^2}$.

(3) Calculate 2D kSZ map follow Eq.(1).

(4) Calculate correlation coefficients.

We compare reconstructed kSZ signals $\hat{\Theta}_{kSZ}$ with kSZ signals Θ_{kSZ} directly from simulations. To quantify the tightness of correlation, we employ a quantity r :

$$r \equiv \frac{P_{recon, real}}{\sqrt{P_{recon} P_{real}}} \quad (4)$$

III. CROSS CORRELATION WITH NOISE SUBTRACTED FIELD

A. Mimic the Noise Subtraction

To resemble realistic observations, we take into account the resolution, small scale noises and foreground subtractions. Two filters are applied on original density contrast δ to imitate the effects of noise subtractions:

1. For small scale noises:

Import a cut off scale k_c with a step function $J(k_c - k)$. For $k > k_c$, $J(k_c - k) = 0$; for $k \leq k_c$, $J(k_c - k) = 1$. This is reasonable for a filled aperture experiment, which has good brightness sensitivity and an exponentially growing noise at small scales. We choose $k_c = 0.5 h/\text{Mpc}$ and $0.32 h/\text{Mpc}$ respectively for $z = 1$ and $z = 2$, which corresponds to $\ell \sim 1150$. This is generally realistic, judging from ongoing 21cm experiments like CHIME [19][28] and Tianlai [29][20].

2. For foreground noises:

Use a high pass filter $W_{fs}(k_{\parallel}) = 1 - e^{-k_{\parallel}^2 R_{\parallel}^2/2}$ to imitate the subtraction. We choose $R_{\parallel} = 15 \text{ Mpc}/h$ for $z = 1$

and $R_{\parallel} = 8 \text{ Mpc}/h$ for $z = 2$, which gives $W_{fs} = 0.5$ at $k_{\parallel} = 0.08 \text{ Mpc}/h$ and $0.15 \text{ Mpc}/h$ respectively.

The observed 21cm field after noises subtraction is then given by

$$\delta_{ns}(\mathbf{k}) = \delta(\mathbf{k})W_{fs}(k_{\parallel})J(k_c - k), \quad (5)$$

With the noise subtracted density contrast δ_{ns} , we follow the procedure described in last section to generate a mock kSZ signal $\hat{\Theta}_{ns}$ and calculate cross correlation $r_{\Theta\hat{\Theta}_{ns}}$.

B. Cross Correlation from Noise Subtracted Field

Fig.1 upper panel Shows the cross correlation between the reconstructed velocity field $\hat{v}_{z,ns}$ and the real velocity field v_z , at redshift 1 and 2.

At this point, all the manipulation and calculation on $\delta(\mathbf{k})$ are independent over different \mathbf{k} , therefore, the cross-correlation closely resembles the subtraction we perform.

Just one interesting thing to notice is that although the foreground at $z=2$ is stronger, the non-linear effects are weaker. So we still can obtain correlations at $k_{\parallel} \lesssim 0.1$ with the seriously suppressed density contrast.

Fig.2 shows the cross correlation between the reconstructed kSZ map $\hat{\Theta}_{ns}$ and real kSZ map Θ at redshift 1 and 2.

There are two points to notice:

(1) For both redshift, there are a considerable amount of correlation $r \gtrsim 0.5$ for $l \gtrsim 1000$; and this correlation drops quickly for smaller l ;

(2) The obtained correlation at redshift 2 is better than redshift 1.

Although not satisfactory at small l , the reconstructed kSZ signal $\hat{\Theta}_{ns}$ from 21cm density field shall already be able to give us reasonable S/N in real applications, because most kSZ signals that can actually be distinguished come from at least $l \gtrsim 500$, when primary CMB gradually dies out.

C. Explanation of the Cross Correlation Behavior

To explain the behavior of the cross correlation, we write Eq.(1) in Fourier space.

$$\Theta(\tilde{\mathbf{k}}_{\perp}) \equiv \Theta(\tilde{k}_x, \tilde{k}_y, 0) \propto \int d^3k \delta(\tilde{\mathbf{k}}_{\perp} - \mathbf{k}_{\perp}, k_{\parallel}) v_z(\mathbf{k})$$

$$\xrightarrow[\text{region}]{\text{linear}} \int d^3k \delta(\tilde{\mathbf{k}}_{\perp} - \mathbf{k}_{\perp}, k_{\parallel}) \delta(\mathbf{k}) \frac{k_z}{k^2} \quad (6)$$

$$\langle \Theta(\tilde{\mathbf{k}}_{\perp}) \Theta^*(\tilde{\mathbf{k}}'_{\perp}) \rangle \propto \int \frac{d^3\mathbf{k}}{(2\pi)^3} \frac{d^3\mathbf{k}'}{(2\pi)^3} \frac{k_z}{k^2} \frac{k'_z}{k'^2}$$

$$\langle \delta(\mathbf{k}) \delta(\tilde{\mathbf{k}}_{\perp} - \mathbf{k}) \delta^*(\mathbf{k}') \delta^*(\tilde{\mathbf{k}}'_{\perp} - \mathbf{k}') \rangle \quad (7)$$

The dominate term is $\langle \delta(\mathbf{k}) \delta^*(\mathbf{k}') \rangle \langle \delta(\tilde{\mathbf{k}}_{\perp} - \mathbf{k}) \delta^*(\tilde{\mathbf{k}}'_{\perp} - \mathbf{k}') \rangle$

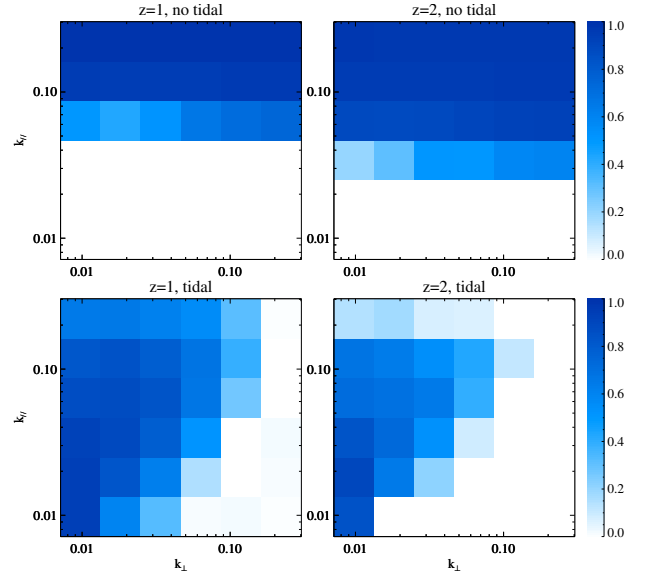


FIG. 1: (Top) The cross correlation r between P_{v_z} and $P_{\hat{v}_{z,ns}}$ calculated from foreground subtracted field δ_{fs} ; (Bottom) The cross correlation between P_{v_z} and $P_{\hat{v}_{z,tide}}$ calculated from $\hat{\kappa}_c$.

and $\langle \delta(\mathbf{k}) \delta^*(\tilde{\mathbf{k}}_{\perp} - \mathbf{k}') \rangle \langle \delta(\tilde{\mathbf{k}}_{\perp} - \mathbf{k}) \delta^*(\mathbf{k}') \rangle$, hence,

$$\langle \Theta(\tilde{\mathbf{k}}_{\perp}) \Theta^*(\tilde{\mathbf{k}}'_{\perp}) \rangle \propto \int d^3k d^3k' \frac{k_z}{k^2} \frac{k'_z}{k'^2}$$

$$P(k) P(\tilde{\mathbf{k}}_{\perp} - \mathbf{k}) [\delta^D(\mathbf{k} - \mathbf{k}') + \delta^D(\mathbf{k} + \mathbf{k}' - \tilde{\mathbf{k}}_{\perp})]$$

$$= \int d^3k \frac{k_z^2}{k^2} P(k) P(\tilde{\mathbf{k}}_{\perp} - \mathbf{k}) \left(\frac{1}{k^2} - \frac{1}{|\tilde{\mathbf{k}}_{\perp} - \mathbf{k}|^2} \right) \quad (8)$$

$$= \int d^3k \ln k \frac{k_z^3 k_x k_y}{k^2} P(k) P(\tilde{\mathbf{k}}_{\perp} - \mathbf{k}) \left(\frac{1}{k^2} - \frac{1}{|\tilde{\mathbf{k}}_{\perp} - \mathbf{k}|^2} \right)$$

We transform $dk \rightarrow d \ln k$ to show the contributions from different k scales. Level of $P(k)$ can be seen in Fig.??

For small $\tilde{k}'_{\perp} = l/\chi \sim 0.01 \text{ h/Mpc}$:

Most $(\frac{1}{k^2} - \frac{1}{|\tilde{\mathbf{k}}_{\perp} - \mathbf{k}|^2}) \sim \frac{1}{k^3}$, so we have $\frac{k_z^3 k_x k_y}{k^5}$ which is scale invariant, and $P(k) P(\tilde{\mathbf{k}}_{\perp} - \mathbf{k})$ reach peak at similar point with small k . Therefore, main contribution of the power spectrum is from large scale. On the other hand, the fields after foreground subtraction lack the part from small k , which caused the null correlation.

For large $\tilde{k}'_{\perp} \sim 1 \text{ h/Mpc}$:

$(\frac{1}{k^2} - \frac{1}{|\tilde{\mathbf{k}}_{\perp} - \mathbf{k}|^2}) \sim \frac{1}{k^2}$ or even $\sim \frac{1}{k^2_{\perp}}$ so we have at least $\frac{k_z^3 k_x k_y}{k^4}$, which prefers small scales. Moreover, $P(k) P(\tilde{\mathbf{k}}_{\perp} - \mathbf{k})$ no longer reach peak at similar point. Therefore, the importance of small k modes is attenuated, and the influence of foregrounds are reduced.

The reason why the correlation on redshift 2 is better is that the density contrast at redshift 1 is sharper than redshift 2, which exaggerates the contribution from small scales.

IV. 3D COSMIC TIDAL RECONSTRUCTION

A. Algorithm

The cosmic tidal reconstruction is a kind of quadratic statistics developed to extract large scale information from alignment of small scale structures. It uses the anisotropic distortions on small scales powerspectrum to solve for the large scale tidal shear and hence gravitational potential.

Here, we present a complete 3 dimensional reconstruction algorithm that works best in close linear regions.

First, we smooth the density contrast to reduce the non-gaussianity.

(1) Convolve the field with a Gaussian kernel $S(\mathbf{k}) = e^{-k^2 R^2/2}$, we take $R = 1.25 \text{ Mpc}/h$ [25], to reduce the complicated non-linear effects on small scales.

(2) Gaussianize the field, taking $\delta_g = \ln(1 + \delta)$. This is to alleviate the problem that filter W_i in Eq.(13) heavily weights high density regions.

Second, we filter for the small scale structures that are most likely to be influenced by tidal force of large scale fields and calculate its variance. With it, we estimate the tidal force and reconstruct the large scale density field.

Consider only second order coupling between small and large scales, the tidal distorted power spectrum [26] is given by

$$P(\mathbf{k}, \tau)|_{t_{ij}} = P_{1s}(k, \tau) + \hat{k}^i \hat{k}^j t_{ij}^{(0)} P_{1s}(k, \tau) f(k, \tau) \quad (9)$$

where $P(\mathbf{k}, \tau)$ can be obtained from observation, $f = 2\alpha(\tau) - \beta(\tau) d \ln P / d \ln k$ describes the theoretical coupling, α and β are functions related to linear growth function [26], and are calculated to be (0.6, 1.3) for $z = 1$ and (0.4, 0.9) for $z = 2$. $P_{1s}(k, \tau)$ is the small scale linear powerspectrum, from theoretical calculation.

(1) Following gravitational lensing procedures, decompose the symmetric, traceless tidal force tensor

$$t_{ij} = \Phi_{L,ij} - \nabla^2 \Phi_L \delta_{ij}^D / 3 \quad (10)$$

into 5 components,

$$t_{ij} = \begin{pmatrix} \gamma_1 - \gamma_z & \gamma_\times & \gamma_2 \\ \gamma_\times & -\gamma_1 - \gamma_z & \gamma_y \\ \gamma_2 & \gamma_y & 2\gamma_z \end{pmatrix}. \quad (11)$$

Here, $\Phi_{L,ij}$ is the second derivative of large scale potential, δ^D is the Dirac function.

(2) Convolve δ_g with a filter W_i deduced from Eq.(9)

$$\delta_g^{w_i}(\mathbf{k}) = W_i(\mathbf{k}) \delta_g(\mathbf{k}) \quad (12)$$

Its effect is to select possible displacements caused by tidal field and calculate the variance.

$$W_i(\mathbf{k}) = i \left(\frac{P(k)f(k)}{P_{tot}^2(k)} \right)^{\frac{1}{2}} \frac{k_i}{k} = S(k) \frac{k_i}{k}$$

where i indicates $\hat{x}, \hat{y}, \hat{z}$ directions, $P_{tot} = P + P_{noise}$ is observed matter powerspectrum, P is theoretical matter powerspectrum,¹

(3) Estimate the 5 tidal tensor components from density variance.

$$\begin{aligned} \hat{\gamma}_1(\mathbf{x}) &= [\delta_g^{w_1}(\mathbf{x}) \delta_g^{w_1}(\mathbf{x}) - \delta_g^{w_2}(\mathbf{x}) \delta_g^{w_2}(\mathbf{x})], \\ \hat{\gamma}_2(\mathbf{x}) &= [2\delta_g^{w_1}(\mathbf{x}) \delta_g^{w_2}(\mathbf{x})], \\ \hat{\gamma}_x(\mathbf{x}) &= [2\delta_g^{w_1}(\mathbf{x}) \delta_g^{w_3}(\mathbf{x})], \\ \hat{\gamma}_y(\mathbf{x}) &= [2\delta_g^{w_2}(\mathbf{x}) \delta_g^{w_3}(\mathbf{x})], \\ \hat{\gamma}_z(\mathbf{x}) &= [(2\delta_g^{w_3}(\mathbf{x}) \delta_g^{w_3}(\mathbf{x}) - \delta_g^{w_1}(\mathbf{x}) \delta_g^{w_1}(\mathbf{x}) - \delta_g^{w_2}(\mathbf{x}) \delta_g^{w_2}(\mathbf{x}))]/3, \end{aligned} \quad (13)$$

(4) Reconstruct large scale density contrast κ_{3D} from tidal tensor:

With Eq.(10) we get $\kappa_{3D} \sim \nabla^2 \Phi_L = \frac{3}{2} \frac{\partial_i \partial_j}{\nabla^2} t_{ij}$, hence

$$\begin{aligned} \kappa_{3D}(\mathbf{k}) &= \frac{1}{k^2} [(k_1^2 - k_2^2) \gamma_1(\mathbf{k}) + 2k_1 k_2 \gamma_2(\mathbf{k}) \\ &\quad + 2k_1 k_3 \gamma_x(\mathbf{k}) + 2k_2 k_3 \gamma_y(\mathbf{k}) \\ &\quad + (2k_3^2 - k_1^2 - k_2^2) \gamma_z(\mathbf{k})]. \end{aligned} \quad (14)$$

Third, we correct bias and suppress noise with a Wiener filter.

Due to the foregrounds, the noise in z direction will be different from x, y direction, therefore we apply an anisotropic Wiener filter.

$$\hat{\kappa}_c(\mathbf{k}) = \frac{\kappa_{3D}(\mathbf{k})}{b(k_\perp, k_\parallel)} W(k_\perp, k_\parallel), \quad (15)$$

Bias $b = \frac{P_{\kappa_{3D}} \delta}{P_\delta}$, Wiener filter $W = \frac{P_\delta}{P_{\kappa_{3D}} / b^2}$.

Here $\hat{\kappa}_c$ is the output large scale density contrast we obtain from tidal reconstruction. We use it to calculate velocity \hat{v}_z^{tide} and mock kSZ signal $\hat{\Theta}_{tide}$ following identical procedure as to noise subtracted field.

B. Cross Correlation from Tidal Reconstructed Field

For comparison, we first present the cross correlation between v_z and \hat{v}_z^{tide} in lower panels of Fig.1.

It is obvious that the previously lost small k_\parallel modes are partly recovered. The reconstruction on k_\parallel direction is better than on k_\perp direction. This is because tidal reconstruction relies heavily on large k modes, yet lots of large k_\perp modes, whose k_\parallel is small, are lost in the foregrounds. There is degrading performance of tidal reconstruction on $z=2$ compared to $z=1$, which mainly results from the stricter cutoff $k_c = 0.32h/Mpc$ compared to $k_c = 0.5h/Mpc$.

In Fig.2, we demonstrate the correlation r between the reconstructed kSZ signal $\hat{\Theta}_{tide}$ and original kSZ signal Θ .

It is important to see: For $z=1$, there are significant improvement on the cross-correlation after tidal reconstruction,

¹ The value of $S(k)$ on different scales could be seen in Appendix 1.

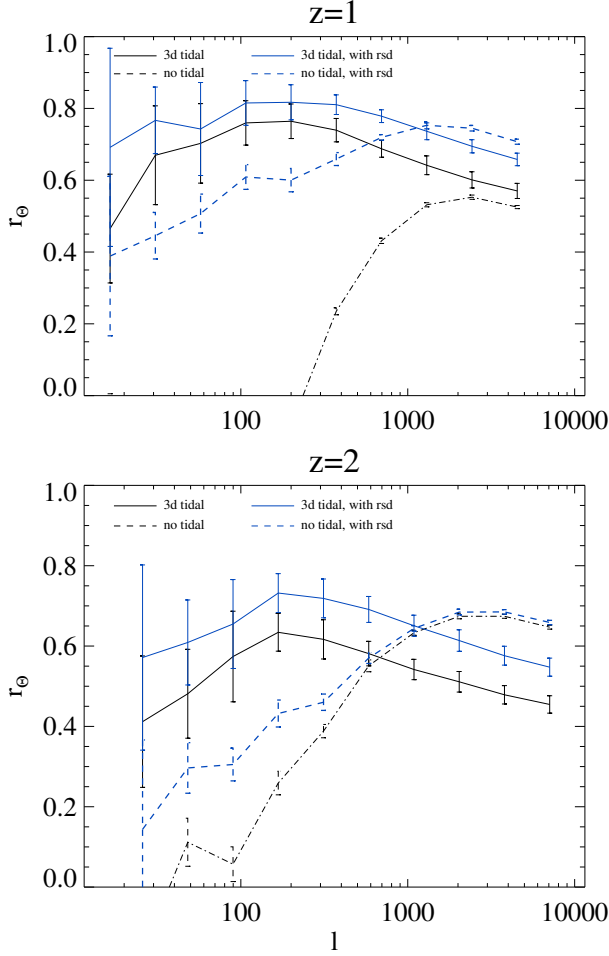


FIG. 2: The cross correlation r between reconstructed kSZ $P_{\Theta_{kSZ}}$ and real kSZ $P_{\Theta_{kSZ}}$. (Dashed line) kSZ calculated from foreground subtracted 21cm density field δ_{fs} ; (Solid line) kSZ calculated from tidal reconstructed density field.

especially below $l \sim 2000$; for $z=2$, the cross-correlation is improved for $l \lesssim 800$. Combining noise subtracted fields and tidal reconstructed fields, we shall have good cross-correlation for $l \sim 50 - 5000$, with the assumed level of foregrounds and noises on small scales.

C. Improvements of Tidal Reconstruction

V. STATISTICAL ERROR

We use the statistical error to estimate the S/N ratio for real surveys, taking into account the contamination from primary CMB and facility noises.

$$\frac{S}{N} = \frac{C_l}{\Delta C_l} \quad (16)$$

$$\simeq r \sqrt{(2l+1)\Delta l f_{sky}} \sqrt{\frac{C_l^{kSZ, \Delta z}}{C_l^{CMB} + C_l^{kSZ} + C_l^{CMB, N}}}$$

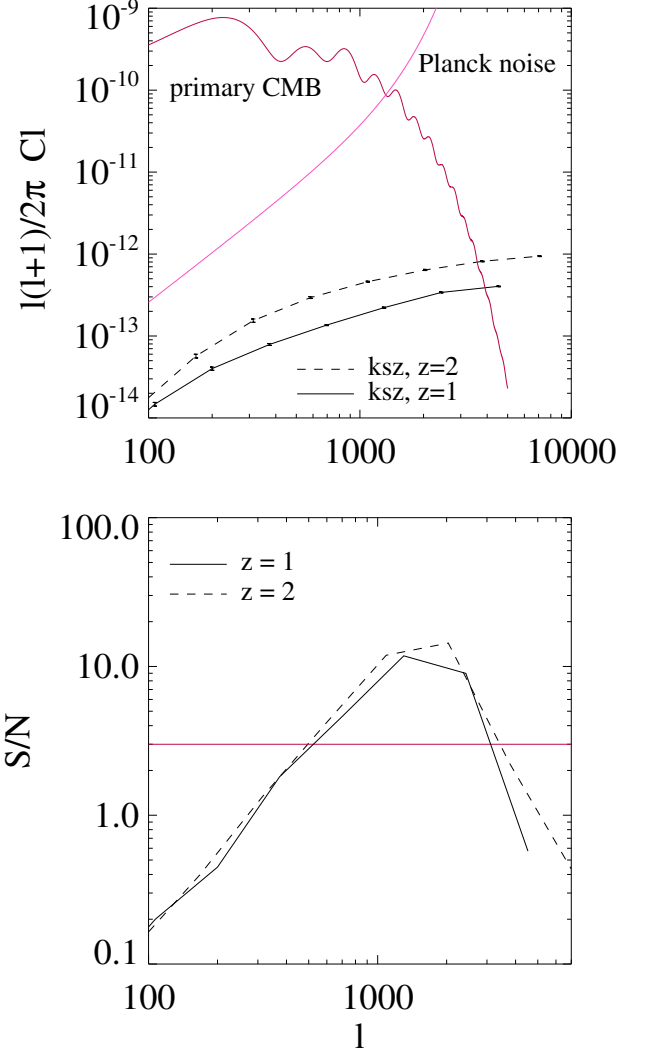


FIG. 3: (Top) Relative strength of kSZ signal, within a box of $\Delta\chi = 1200 \text{ Mpc}/h$. (Bottom) predicted S/N, assuming Planck noise, $\Delta l/l = 0.1$, $f_{sky} = 0.8$.

Where C_l^{CMB} is the angular powerspectrum of primary CMB; $C_l^{CMB, N}$ indicates the facility noises; $C_l^{kSZ, \Delta z}$ is the kSZ signal from a certain redshift bin; r is the correlation coefficients we get; f_{sky} is the percent of sky area covered by both surveys.

In our case, we calculate C_l^{CMB} from CAMB [30]. We use Planck 2015 results [31] at 217GHz to estimate $C_l^{CMB, N}$. $C_l^{CMB, N} = (\sigma_{p,T} \theta_{FWHM})^2 W_l^{-2}$; where $\sigma_{p,T} = 8.7 \mu K_{CMB}$ is Sensitivity per beam solid angle, $\theta_{FWHM} \sim 5'$ is the effective beam FWHM, $W_l = \exp[-l(l+1)/2l_{beam}^2]$ is the smoothing window function, with $l_{beam} = \sqrt{8 \ln 2} / \theta_{FWHM}$. We choose $f_{sky} = 0.8$, since it is feasible for 21cm intensity mapping to survey large sky areas. We choose $\Delta l/l = 0.1$. And for $C_l^{kSZ, \Delta z}$, we choose two bins of size 1200 Mpc/h, centered at redshift 1,2 respectively.

In Fig.3, we plot the S/N level for the two redshift bins. The S/N will exceeds 3 from $l \sim 500 - 3000$.

Since we only use the correlation calculated from tidal recon-

structed field, the S/N shall be higher for $z=2$ combining tidal reconstructed field and foreground subtracted field. Moreover, since C_l^{kSZ} is relatively flat, it is possible to bin it into larger Δl . eg. [18] choose $\Delta l = 200$, and this will yield better S/N for $l < 2000$ in Fig.3.

What's more, Planck's noise level is far from ideal. If we consider the case of 2th generation facilities, there will also be a giant leap for S/N at large l , assuming clean subtraction of CMB lensing.

VI. DISCUSSION AND CONCLUSION

Here is one of the first application of using 3 dimensional tidal reconstruction. When the method is first developed [25][26], it only uses γ_1, γ_2 two shear estimator in x,y plane, concerning the redshift space distortion. However, in our case, the small scale structures in x,y direction are partly lost in foreground subtraction, while large k_z remains more intact, hence most effective parts of reconstruction are coming from the rest three γ that have more contributions from z components. Therefore the 2D tidal reconstruction is definitely insufficient. As for the redshift space distortion, linearly it just induces an additional contraction in z direction $\delta^{rsd}(\mathbf{k}) = (1 + f \frac{k_z^2}{k^2})\delta(\mathbf{k})$. Therefore can be easily subtracted by dividing the additional term before all the calculations. The non-linear effect will not matter much since the large k cutoff we apply will smear the small difference on small scales. (deletable: Actually, even if we do not subtract redshift space distortion, since the foregrounds are also in z direction, the additional term assigns more weight to large k_z modes, where most clean signals come from; assigns more weight to shear estimators related to covariance in

z directions, where best recovered modes come from, and will results to a better reconstruction result (probably discussed in detail in next paper).) Moreover, the inhanement induced by redshift space distortion in large k_z will increase the S/N at that level, therefore improve the reconstruction results. In all, redshift space distortion is not a problem in this case, it is more like a blessing.

In this paper, we discuss the possibility of cross correlating kSZ signal with 21cm intensity mapping as a new probe to study baryon distributions. *yet never mention baryon distribution....* We present the correlation results after foreground subtraction and high k cut off from simulations at redshift 1 and 2. We recover large scale information lost in foregrounds with a 3D tidal reconstruction and obtain a $r > 0.6$ correlation for $l \sim 100 - 2000$, and $S/N > 3$ for $l \sim 500 - 3000$ with Planck noise. This shows a promising future for this method.

VII. ACKNOWLEDGE

We acknowledge discussions with Kendrick Smith, Matthew Johnson, Wenkai Hu, Tianxiang Mao and Jiawei Shao. The simulations were performed on the BGQ supercomputer at the SciNet HPC Consortium. SciNet is funded by: the Canada Foundation for Innovation under the auspices of Compute Canada; the Government of Ontario; the Ontario Research Fund – Research Excellence; and the University of Toronto. Research at the Perimeter Institute is supported by the Government of Canada through Industry Canada and by the Province of Ontario through the Ministry of Research & Innovation. The Dunlap Institute is funded through an endowment established by the David Dunlap family and the University of Toronto.

-
- [1] R. J. Cooke, M. Pettini, R. A. Jorgenson, M. T. Murphy, and C. C. Steidel, *ApJ* **781**, 31 (2014), 1308.3240.
 - [2] G. Hinshaw, D. Larson, E. Komatsu, D. N. Spergel, C. L. Bennett, J. Dunkley, M. R. Nolta, M. Halpern, R. S. Hill, N. Odegard, et al., *ApJS* **208**, 19 (2013), 1212.5226.
 - [3] E. Komatsu, K. M. Smith, J. Dunkley, C. L. Bennett, B. Gold, G. Hinshaw, N. Jarosik, D. Larson, M. R. Nolta, L. Page, et al., *ApJS* **192**, 18 (2011), 1001.4538.
 - [4] G. Hinshaw, D. Larson, E. Komatsu, D. N. Spergel, C. L. Bennett, J. Dunkley, M. R. Nolta, M. Halpern, R. S. Hill, N. Odegard, et al., *ApJS* **208**, 19 (2013), 1212.5226.
 - [5] U.-L. Pen, *ApJ* **510**, L1 (1999), astro-ph/9811045.
 - [6] A. M. Soltan, *A&A* **460**, 59 (2006), astro-ph/0604465.
 - [7] M. Fukugita and P. J. E. Peebles, *ApJ* **616**, 643 (2004), astro-ph/0406095.
 - [8] J. K. Werk, J. X. Prochaska, J. Tumlinson, M. S. Peeples, T. M. Tripp, A. J. Fox, N. Lehner, C. Thom, J. M. O'Meara, A. B. Ford, et al., *ApJ* **792**, 8 (2014), 1403.0947.
 - [9] R. Davé, B. D. Oppenheimer, N. Katz, J. A. Kollmeier, and D. H. Weinberg, *MNRAS* **408**, 2051 (2010), 1005.2421.
 - [10] R. A. Sunyaev and Y. B. Zeldovich, *Comments on Astrophysics and Space Physics* **4**, 173 (1972).
 - [11] R. A. Sunyaev and I. B. Zeldovich, *MNRAS* **190**, 413 (1980).
 - [12] P. Zhang, U.-L. Pen, and H. Trac, *MNRAS* **347**, 1224 (2004), astro-ph/0304534.
 - [13] M. McQuinn, S. R. Furlanetto, L. Hernquist, O. Zahn, and M. Zaldarriaga, *ApJ* **630**, 643 (2005), astro-ph/0504189.
 - [14] O. Zahn, C. L. Reichardt, L. Shaw, A. Lidz, K. A. Aird, B. A. Benson, L. E. Bleem, J. E. Carlstrom, C. L. Chang, H. M. Cho, et al., *ApJ* **756**, 65 (2012), 1111.6386.
 - [15] N. Hand, G. E. Addison, E. Aubourg, N. Battaglia, E. S. Battistelli, D. Bizyaev, J. R. Bond, H. Brewington, J. Brinkmann, B. R. Brown, et al., *Physical Review Letters* **109**, 041101 (2012), 1203.4219.
 - [16] J. Shao, P. Zhang, W. Lin, Y. Jing, and J. Pan, *MNRAS* **413**, 628 (2011), 1004.1301.
 - [17] M. Li, R. E. Angulo, S. D. M. White, and J. Jasche, *MNRAS* **443**, 2311 (2014), 1404.0007.
 - [18] J. C. Hill, S. Ferraro, N. Battaglia, J. Liu, and D. N. Spergel, *ArXiv e-prints* (2016), 1603.01608.
 - [19] K. Bandura, G. E. Addison, M. Amiri, J. R. Bond, D. Campbell-Wilson, L. Connor, J.-F. Cliche, G. Davis, M. Deng, N. Denman, et al., in *Society of Photo-Optical Instrumentation Engineers (SPIE) Conference Series* (2014), vol. 9145 of *Society of Photo-Optical Instrumentation Engineers (SPIE) Conference Series*, p. 22, 1406.2288.
 - [20] Y. Xu, X. Wang, and X. Chen, *ApJ* **798**, 40 (2015), 1410.7794.
 - [21] <http://www.acru.ukzn.ac.za/hirax/>.

- [22] T. Di Matteo, B. Ciardi, and F. Miniati, *MNRAS* **355**, 1053 (2004), astro-ph/0402322.
- [23] K. W. Masui, E. R. Switzer, N. Banavar, K. Bandura, C. Blake, L.-M. Calin, T.-C. Chang, X. Chen, Y.-C. Li, Y.-W. Liao, et al., *ApJ* **763**, L20 (2013), 1208.0331.
- [24] E. R. Switzer, T.-C. Chang, K. W. Masui, U.-L. Pen, and T. C. Voytek, *ApJ* **815**, 51 (2015), 1504.07527.
- [25] U.-L. Pen, R. Sheth, J. Harnois-Déraps, X. Chen, and Z. Li, *ArXiv e-prints* (2012), 1202.5804.
- [26] H.-M. Zhu, U.-L. Pen, Y. Yu, X. Er, and X. Chen, *ArXiv e-prints* (2015), 1511.04680.
- [27] J. Harnois-Déraps, U.-L. Pen, I. T. Iliev, H. Merz, J. D. Emberson, and V. Desjacques, *MNRAS* **436**, 540 (2013), 1208.5098.
- [28] L. B. Newburgh, G. E. Addison, M. Amiri, K. Bandura, J. R. Bond, L. Connor, J.-F. Cliche, G. Davis, M. Deng, N. Denman, et al., in *Society of Photo-Optical Instrumentation Engineers (SPIE) Conference Series* (2014), vol. 9145 of *Society of Photo-Optical Instrumentation Engineers (SPIE) Conference Series*, p. 91454V, 1406.2267.
- [29] X. Chen, *International Journal of Modern Physics Conference Series* **12**, 256 (2012), 1212.6278.
- [30] A. Lewis, A. Challinor, and A. Lasenby, *Astrophys. J.* **538**, 473 (2000), astro-ph/9911177.
- [31] Planck Collaboration, R. Adam, P. A. R. Ade, N. Aghanim, M. Arnaud, M. Ashdown, J. Aumont, C. Baccigalupi, A. J. Banday, R. B. Barreiro, et al., *ArXiv e-prints* (2015), 1502.01587.